Fine Mapping of Bone Structure and Strength QTLs in Heterogeneous Stock Rat

Imranul Alam[a,*], **Daniel L. Koller**[b], **Toni Cañete**[d], **Gloria Blázquez**[d], **Carme Mont-Cardona**[d], **Regina López-Aumatell**[c], **Esther Martínez-Membrives**[d], **Sira Díaz-Morán**[d], **Adolf Tobeña**[d], **Alberto Fernández-Teruel**[d], **Pernilla Stridh**[e], **Margarita Diez**[e], **Tomas Olsson**[e], **Martina Johannesson**[e], **Amelie Baud**[c], **Michael J. Econs**[a,b], and **Tatiana Foroud**[b]

[a]Medicine, Indiana University School of Medicine, IN, USA

[b]Medical and Molecular Genetics, Indiana University School of Medicine, IN, USA

[c]Wellcome Trust Center for Human Genetics, Oxford OX3 7BN, United Kingdom

[d]Department of Psychiatry and Forensic Medicine, Institute of Neurosciences, School of Medicine, Universitat Autònoma de Barcelona, 08193-Bellaterra, Barcelona, Spain

[e]Clinical Neuroscience, Center for Molecular Medicine, Neuroimmunolgy Unit, Karolinska Institutet, S171 76 Stockholm, Sweden

Abstract

We previously demonstrated that skeletal structure and strength phenotypes vary considerably in heterogeneous stock (HS) rats. These phenotypes were found to be strongly heritable, suggesting that the HS rat model represents a unique genetic resource for dissecting the complex genetic etiology underlying bone fragility. The purpose of this study was to identify and localize genes associated with bone structure and strength phenotypes using 1524 adult male and female HS rats between 17 to 20 weeks of age. Structure measures included femur length, neck width, head width; femur and lumbar spine (L3-5) areas obtained by DXA; and cross-sectional areas (CSA) at the midshaft, distal femur and femoral neck, and the 5th lumbar vertebra measured by CT. In addition, measures of strength of the whole femur and femoral neck were obtained. Approximately 70,000 polymorphic SNPs distributed throughout the rat genome were selected for genotyping, with a mean linkage disequilibrium coefficient between neighboring SNPs of 0.95. Haplotypes were estimated across the entire genome for each rat using a multipoint haplotype reconstruction method, which calculates the probability of descent at each locus from each of the 8 HS founder

*Corresponding author: Imranul Alam, PhD, Division of Endocrinology, Indiana University School of Medicine, 1120 W. Michigan St, CL459, Indianapolis, IN 46202, Phone (317) 274-0744, Fax (317) 278-0658, ialam@iu.edu.

Conflict of Interest: All authors have no conflicts of interest.

strains. The haplotypes were then tested for association with each structure and strength phenotype via a mixed model with covariate adjustment. We identified quantitative trait loci (QTLs) for structure phenotypes on chromosomes 3, 8, 10, 12, 17 and 20, and QTLs for strength phenotypes on chromosomes 5, 10 and 11 that met a conservative genome-wide empiric significance threshold (FDR=5%; $P<3 \times 10^{-6}$). Importantly, most QTLs were localized to very narrow genomic regions (as small as 0.3Mb and up to 3 Mb), each harboring a small set of candidate genes, both novel and previously shown to have roles in skeletal development and homeostasis.

Keywords

Heterogeneous stock rat; Bone structure; Bone strength; Genes; Osteoporosis

Introduction

Osteoporosis is a common, genetically complex disorder characterized by reduced bone mineral density (BMD), abnormal bone microarchitecture and compromised bone strength leading to increased susceptibility to fracture risk [1]. Bone mineral density (BMD), structure and strength are the major determinants of skeletal fracture [2-4]. As much as 80% of the variability of BMD and about one-third of the variance in the risk of fracture is due to heritable factors [5-8]. Although BMD by DXA is most often used for predicting fracture risk in humans, it is not an adequate measure to capture several important aspects of bone strength. The genetic basis of fracture susceptibility depends on coordination of bone density, morphology, structure and tissue-quality, all of which contribute to bone strength. Identification and characterization of genes underlying bone structure and strength, particularly at the most common sites of fracture, will ultimately lead to better diagnosis, prevention and treatment of osteoporosis and other high bone-fragility conditions.

Previously, we identified several quantitative trait loci (QTLs) linked to bone structure and strength phenotypes in inbred F344, LEW, COP and DA rats [9-12]. However, most of these QTLs are large (20-30 cM) and harbor hundreds of potential candidate genes. It is a formidable challenge to narrow these critical QTL regions to a small chromosomal segment containing a few genes. To address this issue, in this study we exploited a unique rat model, the heterogeneous stock (HS) rat, developed by the National Institutes of Health (NIH) in 1984 [13]. These rats were derived from eight inbred founder strains: Agouti (ACI/N), Brown Norway (BN/SsN), Buffalo (BUF/N), Fischer 344 (F344/N), M520/N, Maudsley Reactive (MR/N), Wistar-Kyoto (WKY/N) and Wistar-Nettleship (WN/N) [13-14]. Importantly, the descendants of these rats represent a unique, genetically random mosaic of the founding animals' chromosomes due to recombination that has accumulated over 50 generations, enabling the fine mapping of QTLs to very small genomic regions. Recently, these rats have been successfully used for high-resolution mapping for diabetes and fear-related behavior phenotypes [15-16].

In a previous study, we demonstrated that bone structure and strength phenotypes vary considerably among the HS founder strains [17]. Recently, using the sequence data from these strains and genotypes for a dense SNP marker map in the HS offspring population, we

identified several QTLs and underlying genetic variants for multiple bone phenotypes [18]; however, no single genetic variants explaining associations with bone phenotypes were detected, consistent with the complex genetic architecture of skeletal phenotypes observed previously both in humans and animal models [18-19]. The purpose of this study is to identify and localize QTLs for bone structure and strength phenotypes using high-resolution mapping in the HS rat offspring at the most common skeletal fracture sites. We anticipate that using this approach the bone structure and strength QTLs will be localized to much smaller genomic regions than QTLs detected using inbred rat crosses. Ultimately, this will allow us to identify a smaller set of potential candidate genes underlying these QTLs, and contribute to a better understanding of the complex genetic architecture of the fracture risk phenotypes in the rat model and in human.

Materials and Methods

Animals

We used 1524 HS rats (male n=728; female n=796) in this study. The HS rats were bred and grown at the Autonomous University of Barcelona. The rats were housed in cages in pairs (males) and trios (females) and maintained with food and water available ad libitum. The HS rats were raised over 2.5 years in batches of approximately 250 animals in accordance with the Spanish legislation on "Protection of Animals used for Experimental and Other Scientific Purposes" and the European Communities Council Directive (86/609/EEC).

Euthanasia and specimen collection

HS rats were euthanized between 17 and 20 weeks of age by ether inhalation. The lower limbs and lumbar vertebrae (L3-5) were dissected from these animals. The lower limbs on the right side were immediately frozen after harvest wrapped in saline soaked gauge in plastic Ziplock bags at –20°C for subsequent biomechanical testing. To prevent dehydration and any adverse effect on the mechanical properties, we kept the muscle attached to the limbs during the storage period until testing. The lower limbs on the left side and lumbar vertebrae (L3-5) were stripped of muscle, transferred to 70% ethyl alcohol and stored at 4°C for bone structure analyses.

Dual energy X-ray absorptiometry (DXA)

The left femur and lumbar vertebrae 3-5 (L3-5) of the HS rats were scanned using DXA (PIXImus II mouse densitometer; Lunar Corp., Madison, WI, USA) with ultra-high resolution (0.18×0.18 mm/pixel). The machine was calibrated prior to each DXA scanning session using a phantom supplied by the manufacturer. During scanning dissected femurs were positioned with anterior surface facing up and the distal end on left side whereas L3-5 were oriented anterior surface facing up on a standardized platform in air. After completion of the scan of each bone, mutually exclusive region of interest (ROI) boxes were drawn **manually** around the bones from which femur area (mm^2) and lumbar area (mm^2) measurements were obtained. The intra-specimen % coefficient variation for area was less than 1%.

Femur length, femoral head and neck width measurements

The femur size parameters were measured using digital calipers accurate to 0.01 mm, with a precision of ± 0.005 mm (Mitutoyo, Aurora, IL). The femur length (mm) was measured from the end of the medial condyle to the end of the greater trochanter. The maximum transverse diameter (mm) of the femoral head and the shortest transverse distance (mm) of the femoral neck were considered as the width of the femoral head and neck, respectively.

Peripheral quantitative computed tomography (pQCT)

The left femurs were placed in plastic tubes filled with 70% ethyl alcohol and centered in the gantry of a Norland Stratec XCT Research SA+pQCT (Stratec Electronics, Pforzheim, Germany) machine. Single slice measurements of 0.26 mm thickness and a voxel size of 0.07 mm were taken for the femur: one slice through femoral midshaft and one slice approximately 1 mm below the growth plate of distal femur. L5 vertebrae were scanned in cross-section at the caudo-cranial center of the vertebral body. For femoral neck, five consecutive scans perpendicular to the neck axis were obtained 0.25 mm apart from each other starting at the base of the femoral head and ending at the greater trochanter. For each slice, the X-ray source was rotated through 180° of projection. Total (trabecular and cortical) cross-sectional area (CSA; mm^2) from each slice for femur and L5 spine were measured using the thresholds of 500 and 900 **mg/cm^3**. For femoral neck, CSA were measured from the average values of all five slices.

Biomechanical testing

The frozen right femurs were brought to room temperature slowly in a saline bath. The femurs were tested in three-point bending by positioning them with anterior surface facing up and the distal end as close to the left supporting point as possible on the lower supports **(15 mm span for female and 20 mm span for male)** of a three-point bending fixture and applying load at the midpoint using a material testing machine (Alliance RT/5, MTS Systems Corp., Eden Prairie, USA). For femoral neck, the proximal end of the femurs was mounted vertically in a special chuck that clamped the femoral shaft to the lower platen of the same material testing machine. The bones were held in place by a small (1N) preload, and then load was applied directly downward at a crosshead speed of 20 mm/min onto the mid-femur and femoral head at room temperature in monotonic axial compression until fracture. Force and displacement measurements were collected every 0.05 second. From the force vs. displacement curves, we measured the phenotypes that are critical for different aspects of bone fragility - ultimate force (F_u; N), stiffness (S; N/mm), work to failure (W; mJ) and ultimate displacement or elongation (E; mm) in TestWorks software, version 4.06. F_u reflects the strength of the bone or maximum load that the bone can support before failing; S is the slope of the curve represents the bone brittleness; W reflects the amount of energy the specimen can absorb prior to fracture and E is the reciprocal of brittleness. The phenotypes, together, best reflect the clinical aspect of skeletal fragility.

Genotyping

DNA was extracted from liver tissues from 8 original founders and 1524 HS rats using standard protocols. **To reconstruct the genome of each HS rat,** genotypes for over 900,000

SNPs for each rat were selected from an Affymetrix rat custom SNP array (www.affymetrix.com) as described previously [19]. We used only high quality informative (SNP call rate more than 0.99, polymorphic SNPs and no missing genotyping) markers. The average spacing between adjacent SNPs is 12.5 kb, with a maximum gap size of 1 Mb. The maximum density is 15 SNPs in a 10kb window. In addition, there are 19 larger gaps (1-3.8 Mb) on the autosomes (chromosome 1 to chromosome 20) and 12 larger gaps on chromosome X, with a maximum gap of 4.8 Mb. The set of SNPs were pruned to approximately 70,000 high quality SNPs which covered the HS rat genome with a mean linkage disequilibrium coefficient between neighboring SNPs of 0.95.

Measurements of intra- and inter-observer errors

The structure and strength phenotypes were measured in batches consisting approximately 250 samples involving multiple individuals, therefore, we analyzed the intra- (measurement of a phenotype across multiple samples by an individual) and inter-observer (measurement of a phenotype across multiple samples by different individuals) variations for these measurements. We found that the intra-observer % of coefficient of variations (CV) for femur length (<4%), neck width (<13%), head width (<9%), lumbar area (<18%), femur work to failure (<34%), femur elongation (<32%) and femur neck ultimate force (<23%) were comparable to inter-observer variations of these measurements (<6%, <12%, 7%, <16%, <39%, <25% and <20%, respectively), suggesting that the quality of these phenotypic measurements was consistent across all samples in this study.

Statistical genetic analysis

Haplotypes were constructed for each rat across the genome using the multipoint haplotype reconstruction method HAPPY (http://www.well.ox.ac.uk/happy) [20] as described previously [19]. A mixed model approach was employed to test for association between each haplotype and the bone phenotype of interest. Variance components to correct for pedigree relationships were estimated using the EMMA package for the R statistical software [21]. The test for association was conducted for each phenotype via a mixed model, adjusting for age, sex, body weight and batch as described previously [19]. An overall significance threshold of $P < 3 \times 10^{-6}$ ($-\log_{10}P = 5.5$) was used, corresponding to the most stringent of the 5% FDR levels established by permutation for each of the bone structure and strength phenotypes, and applying a Bonferonni correction for the number of traits considered. All models were fitted using the statistical language R (R-Development-Core-Team 2004) [22]. For each QTL meeting the significance threshold, the resampling-based model inclusion probability (RMIP) was obtained as a measure of robustness; QTLs with RMIP values above 0.3 were further explored for candidates of interest. A 95% confidence interval for the position of each QTL detected was obtained as described previously [9,23].

Results

QTL mapping results were obtained throughout the genome for the structural measurements of femur length, neck width, head width and lumbar area (Figure 1A-1D). Results for femur work to failure, elongation and femur neck ultimate force are shown in Figure 1E-1G. Several QTLs reaching the genome-wide FDR and RMIP significance thresholds were

observed in the HS rat sample, and are included in Table 1. Candidate genes within the 95% confidence intervals (CI) for these QTLs are listed in Table 2.

Genome-wide significant association results of femur and femoral neck structure

On chromosome 20 at position 34 Mb, significant linkage was detected for femur length with a –logP value of 6.72 (p=1.9×10^{-7}; Figure 2A and Table 1). The CI for this QTL spanned 2.8 megabase (Mb). On chromosome 8, a QTL was identified which was linked to femur head width with a –logP value of 6.56 (p=2.7×10^{-7}; Figure 2B) spanning less than one megabase. On chromosome 3, a QTL was identified which was linked to femur neck width with a –logP value of 9.75 (p=1.7×10^{-10}; Figure 2C) spanning 2.8 megabase. In addition, a QTL encompassing 0.8 Mb for femur neck width with a –logP value of 8.55 (p=2.7×10^{-9}; Figure 2D) was detected on chromosome 17.

Genome-wide significant association results of lumbar spine structure

The only significant QTL for lumbar area was detected on chromosome 12 at position 22 Mb, with a –logP value of 16.39 (p=4.0×10^{-17}; Figure 3A and 4B) spanning 0.5 Mb chromosomal region.

Genome-wide significant association results of femur and femoral neck strength

We observed two genome-wide significant QTLs for femur strength phenotypes, one each for femur work to failure (Figure 3B and 4A) and femur elongation (Figure 3C) on chromosomes 5 and 11, respectively. The CI for the QTL region on chromosome 5 spans approximately 2.5 Mb whereas the QTL region on chromosome 11 spans 2.9 Mb. In addition, a QTL was identified for femoral neck ultimate force between 46-47 Mb position on chromosome 10 (Figure 3D) spanning 0.3 Mb region. In the same region on chromosome 10, a QTL for femur length was also observed with a significant –logP value of 6.46 (p=3.8×10^{-7}).

Discussion

In this study, we detected and localized QTLs for several key bone structure and strength phenotypes in HS rats at most common skeletal fracture sites. Importantly, most of these loci were localized to very small genomic regions, as small as 0.5 Mb up to 3 Mb, compared to the F2 design used previously for QTL mapping. This approach also allowed us to identify a narrowed list of positional candidate genes underlying each QTL, which can then be analyzed in future functional studies. Such a direct translation from gene identification to functional work is not possible in the traditional F2 design which typically identifies a QTL region harboring hundreds of potential candidate genes.

A critical factor for identification of genes underlying any complex trait such as skeletal fragility is replication of QTLs across studies. If chromosomal regions truly harbor gene/s for a trait, independent studies involving sufficiently large samples will most likely detect the same QTL for that particular trait. Importantly, the genomic resolution of replicated QTLs could be enhanced, thereby narrowing the number of positional candidate genes, by employing a genetically random mosaic model of the founder animals rather than using

traditional two-strain parental crosses. Indeed, several chromosomal regions previously identified in our inbred F2 studies were replicated in HS rats. For example, we detected association with femur work to failure in the HS rats on chromosome 5 (LOD 6.54) (Figure 3B and 4A), which overlapped with multiple QTLs in our F344 X LEW and COP X DA F2 crosses for femur structure and strength phenotypes [10,12]. This QTL in HS rat is syntenic to human chromosome 1p32.2-p33 and close to the location of the tissue-nonspecific ALP gene, which is important for skeletal mineralization. In addition, lumbar area QTL identified in HS rats on chromosome 12 (LOD 16.39) (Figure 3A and 4B) overlapped the QTLs in COP X DA F2 cross for spinal BMD and trabecular area [9,10,58]. This QTL in HS rats is homologous to human chromosome 7q11 (Figure 3A), which was linked to hip and spine BMD and femoral neck geometry [55-57]. Importantly, using HS rats, we were able to fine-map these regions to 1-3 Mb resolution, enabling us to identify a much smaller number of potential candidate genes on these overlapped chromosomes (Table 2). Notably, 2 genes (*Hip1 and Por)* underlying the QTL on chromosome 12 have been previously reported to have important roles in skeletal development and homeostasis. *Hip1*, a member of Huntingtin interactin protein, plays an important role in the clathrin trafficking network. *Hip1* deficient mice have developmental abnormalities and growth defects including severe spinal abnormalities and dwarfism [40,41]. *Por* is the primary electron donor for cytochromes P450. Mutations in *Por* in humans lead to severe malformations including defects in craniofacial and long bones development [42]. In addition, deletion of *Por* recapitulates the human skeletal defects in mouse model, indicating this gene is important for proper bone development [43].

The genes underlying QTLs identified in this study might act alone or in combination to influence bone structure and strength phenotypes in different manner. For example, a single gene might affect multiple bone phenotypes or a cluster of genes may act together to modify a single bone phenotype. Also, the pleiotropic gene/s may contribute not only to different bone phenotypes but also influence phenotypes at different skeletal sites even within a given bone. Indeed, we detected several QTLs in HS rats that overlapped the QTLs in F344 X LEW and COP X DA F2 crosses for different bone phenotypes. The head width QTL in HS rats on chromosome 8 (LOD 6.56) (Figure 2B) overlapped with femur BMD and femoral neck strength QTLs in COP X DA cross [9,10]. The femur length and femur neck ultimate force QTLs identified in HS rats on chromosome 10 (LOD 6.41) (Figure 3D) overlapped the QTLs for spine BMD in both F344 X LEW and COP X DA F2 crosses [9,44]. This region was also coincided with the position of the femur BMC QTL that we reported previously in HS rat [19]. Similarly, the femur length QTL identified in HS rats on chromosome 20 (LOD 6.72) (Figure 2A) overlapped the QTL for femur BMD in COP X DA F2 cross [9]. The QTL region for femoral head width on chromosome 8 in HS rat is syntenic to human chromosome 6q13-14 (Figure 2B). This region was previously linked to osteoarthritis QTL and hand-foot malformation [49,52]. A locus for otosclerosis, a common form of hearing impairment caused by abnormal bone homeostasis of the otic capsule, was mapped to the 6q13-16 region [59]. In addition, 6q14.2-14.3 region harbors gene for cleft lip and palate, a defect of craniofacial development in human [60]. The distal peaks of QTLs for ALP and OC in baboon were mapped close to human orthologous 6q13 region [61]. The femur length QTL on chromosome 10 in HS rat is homologous to the human chromosomes 1q42-44 and

17p11.2 which were linked to rheumatoid arthritis QTL and hip BMD, respectively (Figure 3D) [45,46]. The susceptibility loci for split-hand/foot malformation with long-bone deficiency, a rare severe limb deformity condition were detected at 1q42.2-q43 and 6q14.1 [62]. Furthermore, a locus for Kenny-Caffey syndrome, an osteosclerotic bone dysplasia was identified at 1q42-q43 [63]. Amplification and overexpression of genes in 17p11.2-p12 leads to osteosarcoma [64]. QTLs for developmental components of the craniofacial complex were mapped to baboon ortholog of human chromosome 17p12 [65]. The neck width QTL on chromosome 17 in HS rat is homologous to the human chromosomes 10p12.1-p13, where Paget's disease locus was mapped [66-68]. The QTL for the femur length on chromosome 20 in HS rats is syntenic to 6q21-22 where spine and heel BMD QTLs were detected (Figure 2A) [47,48]. In addition, this human region was linked to osteoarthritis and rheumatoid arthritis QTLs [45,49]. Mutation in a locus of 6q21 harboring OSTM1 gene was found to be linked to human malignant infantile osteopetrosis and craniometaphyseal dysplasia with severe craniofacial involvement shows hmozygosity at 6q21-q22.1 locus in human [69,70]. Among all the genes detected underlying QTL on chromosome 10, several genes have previously shown to play important functions in bone growth and remodeling (Table 2). *Cops3* is an oncogene residing in the human chromosomal region 17p11.2-p12 - the copy number and expression level of *Cops3* was significantly associated with the development of osteosarcoma, the most common primary malignancy of bone [29,30]. *Drg2*, a GTP binding protein, overexpression of which in transgenic mice leads to increased number and activity of osteoclasts and bone loss [31]. *Map2k3* is increased by RANKL, which in turn aids in osteoclastogenesis from bone marrow precursor cells [39]. *Nlrp3*, a member of the NLR family of cytosolic receptors, mediates bone loss at sites of infection by apoptotic cell death of osteoblasts [36]. Mutations in *Nlrp3* are responsible for neonatal-onset multisystem inflammatory disease, exhibiting growth retardation, osteopenia and increased osteoclastogenesis [37], suggesting that this gene is important for postnatal skeletal growth and bone remodeling. *Rai1* encodes a nuclear protein containing a zinc finger homeodomain and regulates cell growth, cell cycle regulation, lipid metabolism, neurological development and behavioral functions [32-33]. Mutation of *Rai* leads to craniofacial and skeletal anomalies (short extremities) in Smith-Magenis syndrome [32]. Both the copy number and expression level of *Rasd1* were significantly associated with the development of osteosarcoma [29]. In addition, using an integrative genetics approach, *Rasd1* was identified as a strong candidate gene for a BMD QTL in mice [34]. *Srebf1* activates genes that regulate lipid biosynthesis, and polymorphism in this gene was found to be associated with a higher risk of osteonecrosis of the femoral head in the Korean population [35]. *Shmt1* and *Top3a* are oncogenes and contribute to the development of osteosarcoma [29,38].

Two novel chromosomal regions linked to bone structure and strength phenotypes were identified in HS rats (Table 1) not found in our F2 studies. On chromosome 3, a QTL was identified for neck width (Figure 2C) and on chromosome 11 we detected a QTL for femur strength (Figure 3C). The QTL region for femoral neck width on chromosome 3 in HS rat is syntenic to human 9q33-34 (Figure 2C), where linkage to neck BMD and osteoarthritis and rheumatoid arthritis QTLs were detected previously [45,50,51]. KBG syndrome, a postnatal short stature, macrodontia, facial and hand anomalies and delayed bone age was associated

with 9q31.2-q33.1 [71]. The femur elongation QTL on chromosome 11 in HS rats is syntenic to human chromosome 3q11-13 and 3q12-26 (Figure 3C), where femur and hip structural QTLs and QTL for rheumatoid arthritis were observed [45,53,54]. QTLs for developmental components of the craniofacial complex were mapped to baboon ortholog of human chromosome 3q11-13 [65]. Three genes (*Gsn, Hspa5* and *Lmx1b)* underlying the QTL on chromosome 3 play important roles in bone and teeth development (Table 2). A haplotype in *Gsn* (gelsolin) was associated with the hip bone phenotypes, and mRNA and protein expressions of *Gsn* in peripheral blood monocytes were lower in female Caucasians with low hip BMD [28]. *Hspa5* (heat shock 70kDa protein 5) or *GRP-78,* an endoplasmic reticulum chaperone protein localized on the plasma membrane in preosteoblasts, is responsible for cellular uptake of Dmp1 for its internalization to the nucleus during bone and tooth development [27]. *Lmx1b* is required for patterning and morphogenesis of the mouse calvaria and is necessary for dorsal-ventral patterning during limb development in mice [24-26].

Several novel genes underlying QTLs discovered in this study were not previously directly linked to any bone phenotype but they code for proteins for various cellular structures and trafficking pathways – such as membrane proteins (*Impg1*, *Senp6*, *Lrrc48*, *Dcbld2*, *Jmjd4* and *Gabrr3*), membrane trafficking (*Gapvd1*, *Llgl1* and *Tom1l2*), cytoskeletal proteins (*Stom*, *Mprip* and *Tom1l2*) and cell junction proteins (*Myo6*, *Myo15a* and *Dcbld2*) that might be important for overall bone homeostasis (Table 2). Also, genes that act as transcription factors or cofactors (*Rhbdd2*, *Zbtb34/43* and *Msl3l2*), G-protein coupled receptors (*Gpr15*, *Mprip*, *Myo6* and *Myo15a*), small GTPase (*Arl6* and *Arl5b*) and calcium binding proteins (*Flii* and *Fkbp6*) were identified (Table 2). These genes might play role in connection between skeletal metabolism and other systems functions.

There are some limitations in this study. Although, rat skeleton is very similar to human bone with peak bone mass gain or bone loss due to aging, and rat models have served as a highly predictive model for fracture risk in humans, a potential drawback is rat skeleton lacks the Haversian remodeling system found in human. Also, we could not identify any specific sequence variants in the HS founder strains that fully accounted for structure and strength QTLs identified in this study. In the future, full sequence information of HS offspring will shed light on the complex genetic interactions among the different haplotype variants underlying these phenotypes in these animals. Furthermore, while QTLs for bone structure and strength phenotypes in the HS rat were localized to very small genomic regions, further functional studies are necessary to identify the causative genes from these narrowed lists of candidate genes.

In this study, we demonstrated that HS rats are a powerful resource for fine mapping of QTLs for bone structure and strength phenotypes. These phenotypes, along with BMD, are complex in nature in the rat, just as they are in humans and are likely due to multiple variants inherited from different founders as well as interactions among these variants. The number of founder rat lines used in the generation of the HS population and the number of recombination events accumulated over many generations, allowed us to more accurately detect the correct QTL position. Most importantly, this approach allows us to delineate a much smaller chromosomal QTL interval and thus generate a narrower list of potential

candidate genes than the traditional F2 approach – which is a cross of only two founder rat lines. In the future, sequencing studies in the HS offspring in these narrowed regions, along with analysis of the founder strain sequence data, will enable us to dissect the complex genetic architecture underlying the structure and strength phenotypes in the HS rats.

Acknowledgments

References

1. Rachner TD, Khosla S, Hofbauer LC. Osteoporosis: now and the future. Lancet. 2011; 377:1276–87. [PubMed: 21450337]

2. Cummings SR, Black DM, Nevitt MC, et al. Bone density at various sites for prediction of hip fractures. The Study of Osteoporotic Fractures Research Group. Lancet. 1993; 341:72–75. [PubMed: 8093403]

3. Faulkner KG, Cummings SR, Black D, Palermo L, Gluer CC, Genant HK. Simple measurement of femoral geometry predicts hip fracture: the study of osteoporotic fractures. J Bone Miner Res. 1993; 8:1211–17. [PubMed: 8256658]

4. Peacock M, Turner CH, Liu G, Manatunga AK, Timmerman L, Johnston CC Jr. Better discrimination of hip fracture using bone density, geometry and architecture. Osteoporos Int. 1995; 5:167–73. [PubMed: 7655177]

5. Arden NK, Baker J, Hogg C, Bann K, Spector TD. The heritability of bone mineral density, ultrasound of the calcaneus and hip axis length: a study of postmenopausal twins. J Bone Miner Res. 1996; 11:530–34. [PubMed: 8992884]

6. Garnero P, Arden NK, Griffiths G, Delmas PD, Spector TD. Genetic influence on bone turnover in postmenopausal twins. J Clin Endocrinol Metab. 1996; 81:140–46. [PubMed: 8550741]

7. Peacock M, Turner CH, Econs MJ, Foroud T. Genetics of osteoporosis. Endocr Rev. 2002; 23:378–83.

8. Ralston SH. Genetic determinants of osteoporosis. Curr Opin Rheumatol. 2005; 17:475–79. [PubMed: 15956846]

9. Alam I, Sun Q, Liu L, et al. Sex-specific genetic loci for femoral neck bone mass and strength identified in inbred COP and DA rats. J Bone Miner Res. 2008; 23:850–59. [PubMed: 18282130]

10. Sun Q, Alam I, Liu L, et al. Genetic loci affecting bone structure and strength in inbred COP and DA rats. Bone. 2008; 42:547–53. [PubMed: 18158281]

11. Alam I, Sun Q, Liu L, et al. Identification of a quantitative trait locus on rat chromosome 4 that is strongly linked to femoral neck structure and strength. Bone. 2006; 39:93–99. [PubMed: 16461031]

12. Alam I, Sun Q, Liu L, et al. Whole-genome scan for linkage to bone strength and structure in inbred Fischer 344 and Lewis rats. J Bone Miner Res. 2005; 20:1589–96. [PubMed: 16059631]

13. Hansen C, Spuhler K. Development of the National Institutes of Health genetically heterogeneous rat stock. Alcohol Clin Exp Res. 1984; 8:477–9. [PubMed: 6391259]

14. Boucher W, Cotterman CW. On the classification of regular systems of inbreeding. J Math Biol. 1990; 28:293–305. [PubMed: 2332706]

15. Solberg Woods LC, Holl K, Tschannen M, Valdar W. Fine-mapping a locus for glucose tolerance using heterogeneous stock rats. Physiol Genomics. 2010; 41:102–8. [PubMed: 20068026]

16. Johannesson M, Lopez-Aumatell R, Stridh P, et al. A resource for the simultaneous high-resolution mapping of multiple quantitative trait loci in rats: the NIH heterogeneous stock. Genome Res. 2009; 19:150–8. [PubMed: 18971309]

17. Alam I, Koller DL, Sun Q, et al. Heterogeneous stock rat: A unique animal model for mapping genes influencing bone fragility. Bone. 2011; 48:1169–1177. [PubMed: 21334473]

18. Baud A, Hermsen R, Guryev V, et al. Combined sequence-based and genetic mapping analysis of complex traits in outbred rats. Nat Genet. 2013; 45(7):767–75. [PubMed: 23708188]

19. Alam I, Koller DL, Cañete T, et al. High-Resolution Genome Screen for Bone Mineral Density in Heterogeneous Stock Rat. J Bone Miner Res. Feb 12.2014 doi: 10.1002/jbmr.2195.

20. Mott R, Talbot CJ, Turri MG, Collins AC, Flint J. A method for fine mapping quantitative trait loci in outbred animal stocks. Proc Natl Acad Sci USA. 2000; 97:12649–54. [PubMed: 11050180]

21. Kang HM, Zaitlen NA, Wade CM, et al. Efficient control of population structure in model organism association mapping. Genetics. 2008; 178(3):1709–23. [PubMed: 18385116]

22. R. Development Core Team. R: A language and environment for statistical computing. R Foundation for Statistical Computing; Vienna, Austria: 2004.

23. Visscher PM, Thompson R, Haley CS. Confidence intervals in QTL mapping by bootstrapping. Genetics. 1996; 143(2):1013–20. [PubMed: 8725246]

24. Chen H, Ovchinnikov D, Pressman CL, Aulehla A, Lun Y, Johnson RL. Multiple calvarial defects in lmx1b mutant mice. Dev Genet. 1998; 22(4):314–20. [PubMed: 9664684]

25. Chen H, Johnson RL. Interactions between dorsal-ventral patterning genes lmx1b, engrailed-1 and wnt-7a in the vertebrate limb. Int J Dev Biol. 2002; 46(7):937–41. [PubMed: 12455631]

26. Feenstra JM, Kanaya K, Pira CU, Hoffman SE, Eppey RJ, Oberg KC. Detection of genes regulated by Lmx1b during limb dorsalization. Dev Growth Differ. 2012; 54(4):451–62. [PubMed: 22417325]

27. Ravindran S, Narayanan K, Eapen AS, et al. Endoplasmic reticulum chaperone protein GRP-78 mediates endocytosis of dentin matrix protein 1. J Biol Chem. 2008; 283(44):29658–70. [PubMed: 18757373]

28. Deng FY, Zhu W, Zeng Y, et al. Is GSN significant for hip BMD in female Caucasians? Bone. 2014; 63:69–75. [PubMed: 24607942]

29. Both J, Wu T, Bras J, Schaap GR, Baas F, Hulsebos TJ. Identification of novel candidate oncogenes in chromosome region 17p11.2-p12 in human osteosarcoma. PLoS One. 2012; 7(1):e30907. [PubMed: 22292074]

30. Yan T, Wunder JS, Gokgoz N, et al. COPS3 amplification and clinical outcome in osteosarcoma. Cancer. 2007; 109(9):1870–6. [PubMed: 17366602]

31. Ke K, Sul OJ, Kim WK, et al. Overexpression of developmentally regulated GTP-binding protein-2 increases bone loss. Am J Physiol Endocrinol Metab. 2013; 304(7):E703–1. [PubMed: 23360825]

32. Dubourg C, Bonnet-Brilhault F, Toutain A, et al. Identification of Nine New RAI1-Truncating Mutations in Smith-Magenis Syndrome Patients without 17p11.2 Deletions. Mol Syndromol. 2014; 5(2):57–64. [PubMed: 24715852]

33. Williams SR, Aldred MA, Der Kaloustian VM, et al. Haploinsufficiency of HDAC4 causes brachydactyly mental retardation syndrome, with brachydactyly type E, developmental delays, and behavioral problems. Am J Hum Genet. 2010; 87(2):219–28. [PubMed: 20691407]

34. Farber CR, van Nas A, Ghazalpour A, et al. An integrative genetics approach to identify candidate genes regulating BMD: combining linkage, gene expression, and association. J Bone Miner Res. 2009; 24(1):105–16. [PubMed: 18767929]

35. Lee HJ, Choi SJ, Hong JM, et al. Association of a polymorphism in the intron 7 of the SREBF1 gene with osteonecrosis of the femoral head in Koreans. Ann Hum Genet. 2009; 73(1):34–41. [PubMed: 19040658]

36. Bonar SL, Brydges SD, Mueller JL, et al. Constitutively activated NLRP3 inflammasome causes inflammation and abnormal skeletal development in mice. PLoS One. 2012; 7(4):e35979. [PubMed: 22558291]

37. McCall SH, Sahraei M, Young AB, et al. Osteoblasts express NLRP3, a nucleotide-binding domain and leucine-rich repeat region containing receptor implicated in bacterially induced cell death. J Bone Miner Res. 2008; 23(1):30–40. [PubMed: 17907925]

38. van Dartel M, Cornelissen PW, Redeker S, et al. Amplification of 17p11.2 approximately p12, including PMP22, TOP3A, and MAPK7, in high-grade osteosarcoma. Cancer Genet Cytogenet. 2002; 139(2):91–6. [PubMed: 12550767]

39. Huang H, Ryu J, Ha J, et al. Osteoclast differentiation requires TAK1 and MKK6 for NFATc1 induction and NF-kappaB transactivation by RANKL. Cell Death Differ. 2006; 13(11):1879–91. [PubMed: 16498455]

40. Hyun TS, Li L, Oravecz-Wilson KI, et al. Hip1-related mutant mice grow and develop normally but have accelerated spinal abnormalities and dwarfism in the absence of HIP1. Mol Cell Biol. 2004; 24(10):4329–40. [PubMed: 15121852]

41. Oravecz-Wilson KI, Kiel MJ, Li L, et al. Huntingtin Interacting Protein 1 mutations lead to abnormal hematopoiesis, spinal defects and cataracts. Hum Mol Genet. 2004; 13(8):851–67. [PubMed: 14998932]

42. Panda SP, Guntur AR, Polusani SR, et al. Conditional deletion of cytochrome p450 reductase in osteoprogenitor cells affects long bone and skull development in mice recapitulating antley-bixler syndrome: role of a redox enzyme in development. PLoS One. 2013; 8(9):e75638. [PubMed: 24086598]

43. Wudy SA, Hartmann MF, Draper N, Stewart PM, Arlt W. A male twin infant with skull deformity and elevated neonatal 17-hydroxyprogesterone: a prismatic case of P450 oxidoreductase deficiency. Endocr Res. 2004; 30(4):957–64. [PubMed: 15666853]

44. Koller DL, Alam I, Sun Q, et al. Genome screen for bone mineral density phenotypes in Fischer 344 and Lewis rats. Mammalian Genome. 2005; 16:578–86. [PubMed: 16180139]

45. Jawaheer D, Seldin MF, Amos CI, et al. A genomewide screen in multiplex rheumatoid arthritis families suggests genetic overlap with other autoimmune diseases. Am J Hum Genet. 2001; 68(4): 927–36. [PubMed: 11254450]

46. Deng HW, Xu FH, Huang QY, et al. A whole-genome linkage scan suggests several genomic regions potentially containing quantitative trait Loci for osteoporosis. J Clin Endocrinol Metab. 2002; 87(11):5151–9. [PubMed: 12414886]

47. Karasik D, Myers RH, Cupples LA, et al. Genome screen for quantitative trait loci contributing to normal variation in bone mineral density: the Framingham Study. J Bone Miner Res. 2002; 17(9): 1718–27. [PubMed: 12211443]

48. Moayyeri A, Hsu YH, Karasik D, et al. Genetic determinants of heel bone properties: genome-wide association meta-analysis and replication in the GEFOS/GENOMOS consortium. Hum Mol Genet. 2014; 23(11):3054–68. [PubMed: 24430505]

49. Loughlin J, Mustafa Z, Irven C, et al. Stratification analysis of an osteoarthritis genome screen-suggestive linkage to chromosomes 4, 6, and 16. Am J Hum Genet. 1999; 65(6):1795–8. [PubMed: 10577938]

50. Ioannidis JP, Ng MY, Sham PC, et al. Meta-analysis of genome-wide scans provides evidence for sex- and site-specific regulation of bone mass. J Bone Miner Res. 2007; 22(2):173–83. [PubMed: 17228994]

51. Leppävuori J, Kujala U, Kinnunen J, et al. Genome scan for predisposing loci for distal interphalangeal joint osteoarthritis: evidence for a locus on 2q. Am J Hum Genet. 1999; 65(4): 1060–7. [PubMed: 10486325]

52. Naveed M, Nath SK, Gaines M, et al. Genomewide linkage scan for split-hand/foot malformation with long-bone deficiency in a large Arab family identifies two novel susceptibility loci on chromosomes 1q42.2-q43 and 6q14.1. Am J Hum Genet. 2007; 80(1):105–11. [PubMed: 17160898]

53. Koller DL, Liu G, Econs MJ, et al. Genome screen for quantitative trait loci underlying normal variation in femoral structure. J Bone Miner Res. 2001; 16(6):985–91. [PubMed: 11393795]

54. Koller DL, White KE, Liu G, et al. Linkage of structure at the proximal femur to chromosomes 3, 7, 8, and 19. J Bone Miner Res. 2003; 18(6):1057–65. [PubMed: 12817759]

55. Tang ZH, Xiao P, Lei SF, et al. A bivariate whole-genome linkage scan suggests several shared genomic regions for obesity and osteoporosis. J Clin Endocrinol Metab. 2007; 92(7):2751–7. [PubMed: 17473065]

56. Lei S, Deng F, Xiao P, et al. Bivariate whole-genome linkage scan for bone geometry and total body fat mass. J Genet Genomics. 2009; 36(2):89–97. [PubMed: 19232307]

57. Huang QY, Xu FH, Shen H, et al. A second-stage genome scan for QTLs influencing BMD variation. Calcif Tissue Int. 2004; 75(2):138–43. [PubMed: 15085314]

58. Koller DL, Liu L, Alam I, et al. Linkage screen for BMD phenotypes in male and female COP and DA rat strains. J Bone Miner Res. 2008; 23(9):1382–8. [PubMed: 18707222]

59. Thys M, Van Den Bogaert K, Iliadou V, et al. A seventh locus for otosclerosis, OTSC7, maps to chromosome 6q13-16.1. Eur J Hum Genet. 2007; 15(3):362–8. [PubMed: 17213839]

60. Letra A, Menezes R, Fonseca RF, et al. Novel cleft susceptibility genes in chromosome 6q. J Dent Res. 2010; 89(9):927–32. [PubMed: 20511563]

61. Havill LM, Rogers J, Cox LA, Mahaney MC. QTL with pleiotropic effects on serum levels of bone-specific alkaline phosphatase and osteocalcin maps to the baboon ortholog of human chromosome 6p23-21.3. J Bone Miner Res. 2006; 21(12):1888–96. [PubMed: 17002583]

62. Naveed M, Nath SK, Gaines M, et al. Genome wide linkage scan for split-hand/foot malformation with long-bone deficiency in a large Arab family identifies two novel susceptibility loci on chromosomes 1q42.2-q43 and 6q14.1. Am J Hum Genet. 2007; 80(1):105–11. [PubMed: 17160898]

63. Diaz GA, Khan KT, Gelb BD. The autosomal recessive Kenny-Caffey syndrome locus maps to chromosome 1q42-q43. Genomics. 1998; 54(1):13–8. [PubMed: 9806825]

64. van Dartel M, Hulsebos TJ. Amplification and overexpression of genes in 17p11.2 ~ p12 in osteosarcoma. Cancer Genet Cytogenet. 2004; 153(1):77–80. [PubMed: 15325100]

65. Sherwood RJ, Duren DL, Havill LM, et al. A genomewide linkage scan for quantitative trait loci influencing the craniofacial complex in baboons (Papio hamadryas spp.). Genetics. 2008; 180(1): 619–28. [PubMed: 18757921]

66. Ralston SH, Albagha OM. Genetics of Paget's disease of bone. Curr Osteoporos Rep. 2014; 12(3): 263–71. [PubMed: 24988994]

67. Lucas GJ, Riches PL, Hocking LJ, et al. Identification of a major locus for Paget's disease on chromosome 10p13 in families of British descent. J Bone Miner Res. 2008; 23(1):58–63. [PubMed: 17907922]

68. Hocking LJ, Herbert CA, Nicholls RK, et al. Genomewide search in familial Paget disease of bone shows evidence of genetic heterogeneity with candidate loci on chromosomes 2q36, 10p13, and 5q35. Am J Hum Genet. 2001; 69(5):1055–61. [PubMed: 11555792]

69. Ramírez A, Faupel J, Goebel I, et al. Identification of a novel mutation in the coding region of the grey-lethal gene OSTM1 in human malignant infantile osteopetrosis. Hum Mutat. 2004; 23(5): 471–6. [PubMed: 15108279]

70. Prontera P, Rogaia D, Sobacchi C, et al. Craniometaphyseal dysplasia with severe craniofacial involvement shows homozygosity at 6q21-22.1 locus. Am J Med Genet A. 2011; 155A(5):1106–8. [PubMed: 21465646]

71. Xu M, Zhou H, Yong J, et al. A Chinese patient with KBG syndrome and a 9q31.2-33.1 microdeletion. Eur J Med Genet. 2013; 56(5):245–50. [PubMed: 23369839]

Highlights

• We detected QTLs for bone structure and strength phenotypes in HS rats at the most common skeletal fracture sites

• Several chromosomal regions previously identified in our inbred F2 cross were replicated in HS rats

• Most QTLs in HS rats were localized to very narrow genomic regions

• HS rat model allowed us to identify a narrower list of potential candidate genes than the traditional F2 approach

• We demonstrated that HS rats are a powerful resource for fine mapping of QTLs for bone structure and strength phenotypes
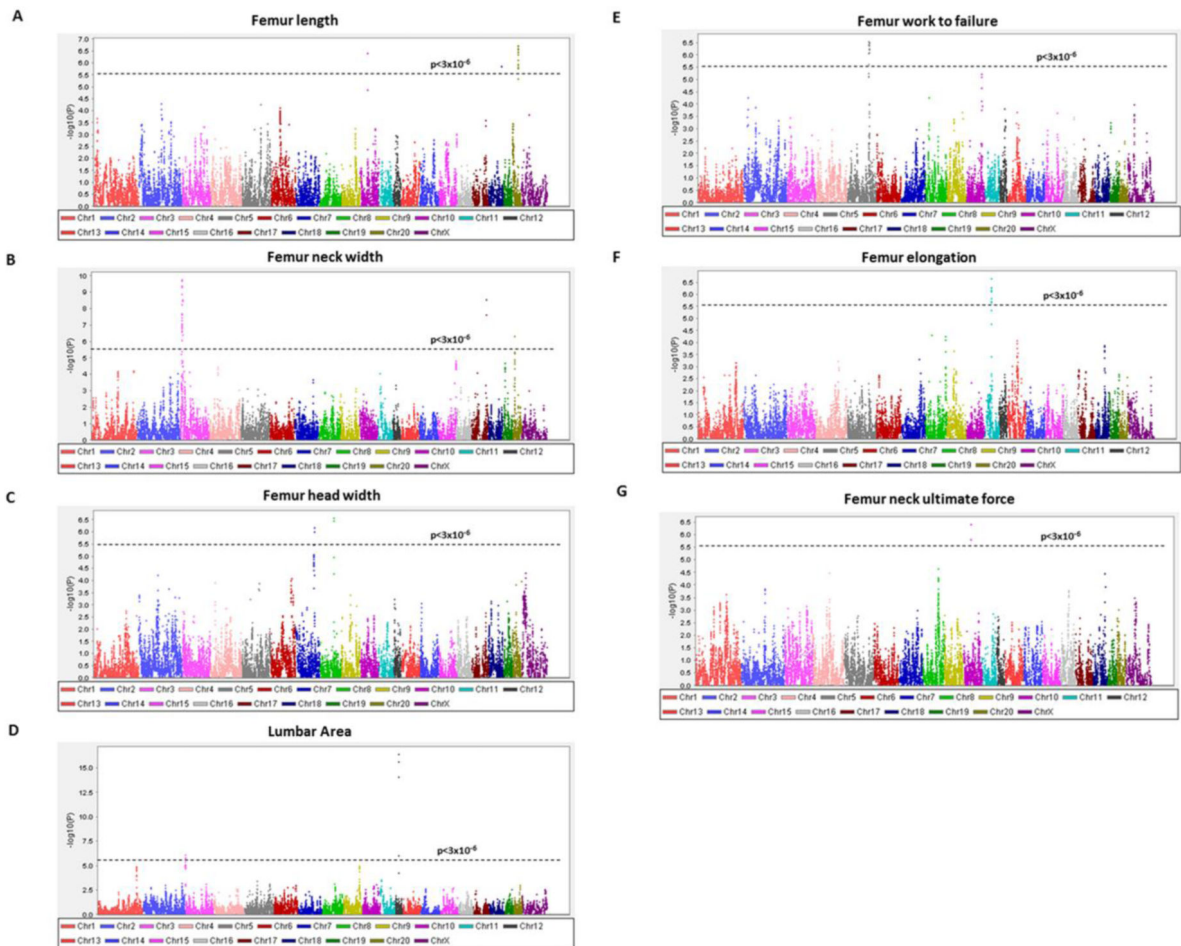
Fig. 1.
Genome-wide plots for femur length (A), femur neck width (B), femur head width (C), lumbar area (D), femur work to failure (E), femur elongation (F), and femur neck ultimate force (G). The –log10P values plotted on the Y-axis versus chromosome position on the X-axis. For comparability with other mapping studies, QTL results are shown at each position regardless of the conservative RMIP threshold (0.3) employed to select the most robust QTLs for our report. The dashed horizontal lines indicate the threshold value for genome-wide significance corresponding to FDR=5% ($p < 3 \times 10^{-6}$).
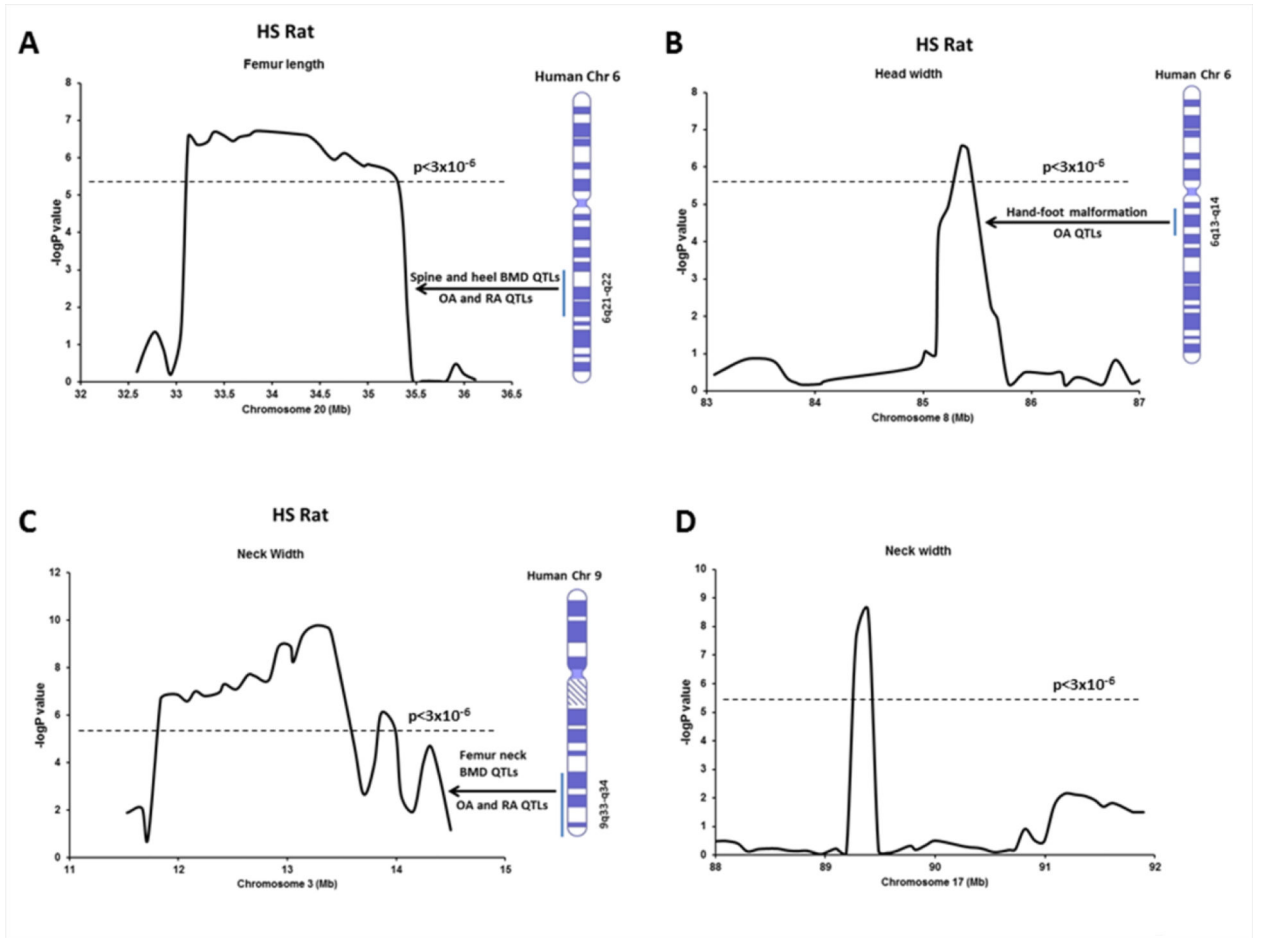
Fig. 2.
Association results for femur length on chromosome 20 (A), femur head width on chromosome 8 (B), femoral neck width on chromosome 3 (C) and femoral neck width on chromosome 17 (D). The –logP values are plotted on the Y-axis vs. the chromosomal position (MB) on the X-axis. The dashed horizontal lines indicate the threshold value for genome-wide significance corresponding to FDR=5% ($p < 3 \times 10^{-6}$). Corresponding human syntenic regions and associated QTLs for bone phenotypes are indicated.
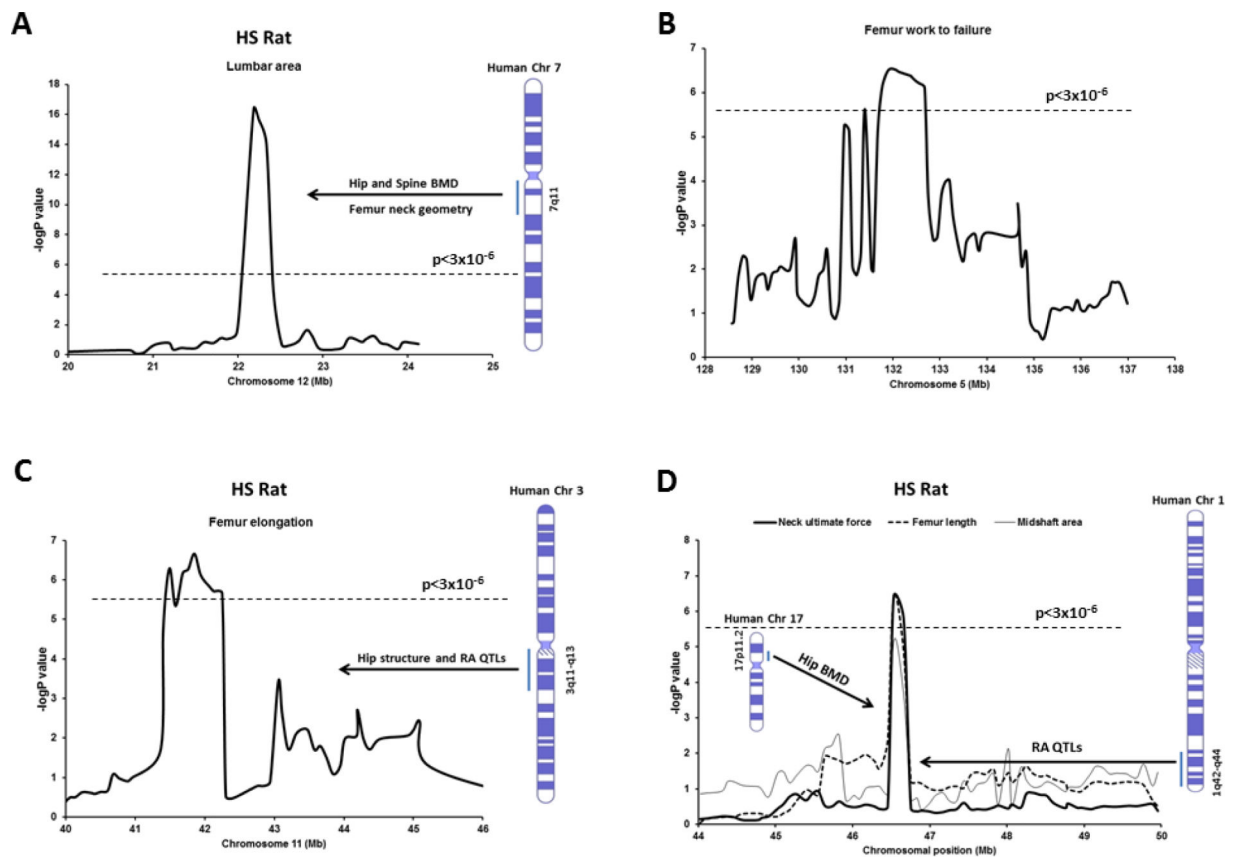
Fig. 3.
Association results for lumbar area on chromosome 12 (A), femur work to failure on chromosome 5 (B), femur elongation on chromosome 11 (C), and femoral neck ultimate force, femur length and midshaft area on chromosome 10 (D). The –logP values are plotted on the Y-axis vs. the chromosomal position (MB) on the X-axis. The dashed horizontal lines indicate the threshold value for genome-wide si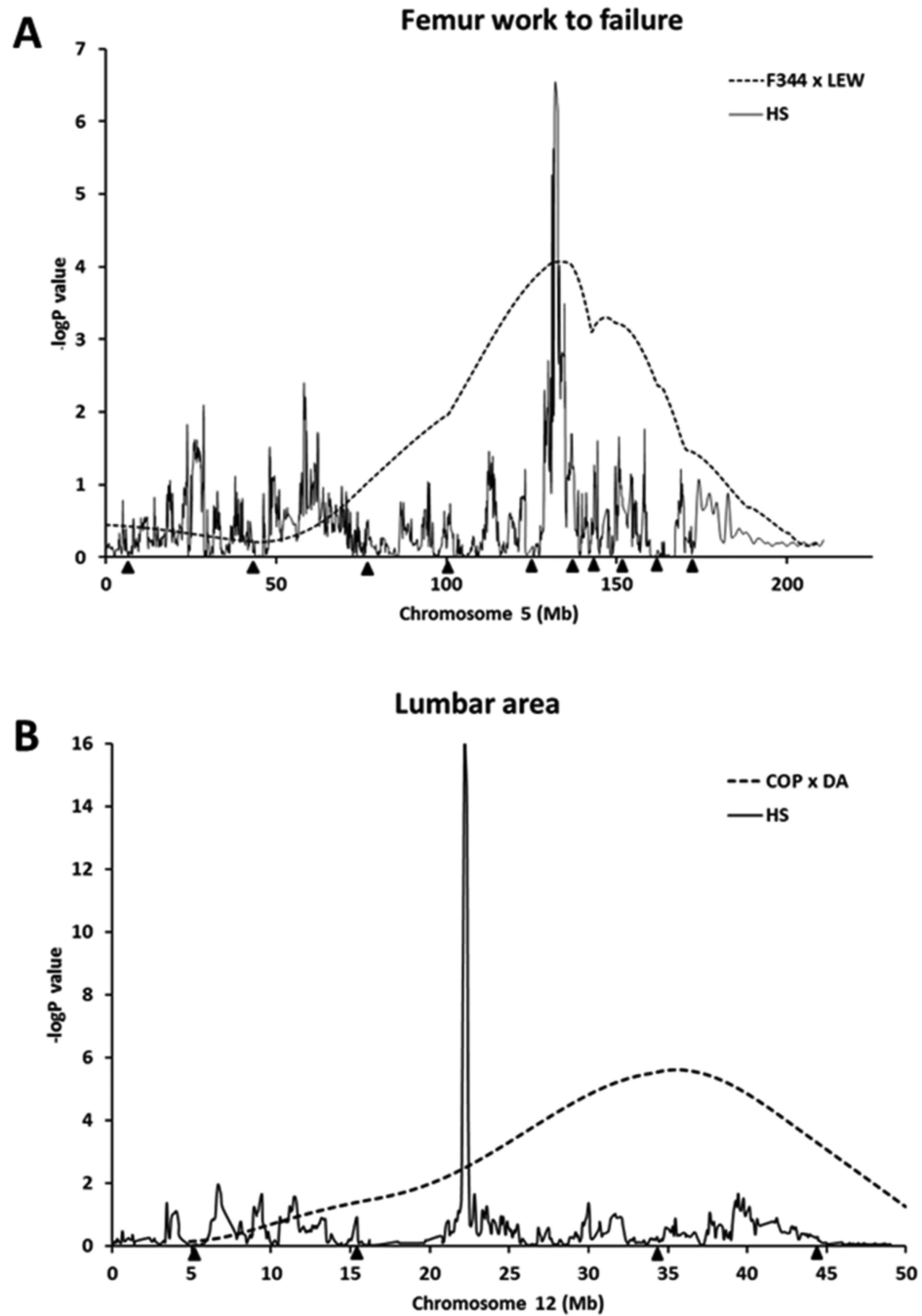gnificance corresponding to FDR=5% ($p < 3 \times 10^{-6}$). Corresponding human syntenic regions and associated QTLs for bone phenotypes are indicated.

Fig. 4.
Mapping results on chromosome 5 (A) for femur work to failure and on chromosome 12 (B) for lumbar area, indicating evidence for QTLs from the HS analysis (solid line) and an F2 intercross (F344 X LEW or COP X DA) reported previously (dotted line). Black triangles along the x-axis correspond to the positions of microsatellite markers typed on each chromosome for the particular F2 intercross.

Table 1

Chromosomal regions associated with significant linkage ($p < 3 \times 10^{-6}$) for bone structure and strength phenotypes

Phenotypes	Chromosome	Position (bp)	Interval (Mb)	P-value	logP
Neck width (mm)	3	13253530	12.2 - 15.0	1.75E-10	9.757
Femur work to failure (mJ)	5	131940562	131.0 - 133.5	2.87E-07	6.542
Head width (mm)	8	85352278	84.9 - 85.8	2.71E-07	6.567
Femur length (mm)	10	46530592	45.7 - 47.1	3.84E-07	6.416
Femur neck ultimate force (N)	10	46530592	46.4 - 46.9	3.89E-07	6.410
Femur elongation (mm)	11	41851716	41.4 - 44.3	2.20E-07	6.658
Lumbar area (mm^2)	12	22185260	22.0 - 22.5	4.00E-17	16.398
Neck width (mm)	17	89388214	89.0 - 89.8	2.78E-09	8.556
Femur length (mm)	20	33840664	32.6 - 35.4	1.90E-07	6.721

Table 2

Candidate genes within the chromosomal locations with significant ($p<3 \times 10^{-6}$) associations for bone structure and strength phenotypes

Phenotype	Chromosome	Interval (Mb)	Gene symbol	Gene name	Human synteny
Neck width (mm)	3	12.2 - 15.0	*Angptl2*	Angiopoietin-related protein 2	9q31-q34.11
			Cntr1	Centriolin	
			Dab2ip	Disabled homolog 2-interacting protein	
			Fbxw2	F-box/WD repeat-containing protein 2	
			Gapvd1	GTPase activating protein and VPS9 domains 1	
			Ggta1	Glycoprotein alpha-galactosyltransferase 1	
			Ggta1l1	Glycoprotein alpha-galactosyltransferase 1-like 1	
			Gsn	Gelsolin	
			Hspa5	78 kDa glucose-regulated protein	
			Lmx1b	Homeodomain protein LMX1b	
			Mapkap1	Target of rapamycin complex 2 subunit MAPKAP1	
			Pbx3	Pre-B-cell leukemia transcription factor 3	
			Phf19	PHD finger protein 19	
			Psmd5	26S proteasome non-ATPase regulatory subunit 5	
			Rab14	Ras-related protein Rab-14	
			Rabepk	Rab9 effector protein with kelch motifs	
			Stom	Erythrocyte band 7 integral membrane protein	
			Zbtb34/43	Zinc finger and BTB domain-containing protein 34/43	
Femur work to failure (mJ)	5	131.0 - 133.5	*Agbl4*	ATP/GTP binding protein-like 4	1p32.2-p33
			Bend5	BEN domain containing 5	
			Cdkn2c	Cyclin-dependent kinase inhibitor 2C (p18 inhibits CDK4)	
			Dmrta2	DMRT-like family A2	
			Elavl4	ELAV (embryonic lethal abnormal vision Drosophila)-like 4	
			Faf1	Fas (TNFRSF6) associated factor 1	
			Skint8	Selection and upkeep of intraepithelial T cells 8	
			Slc5a9	Solute carrier family 5 (sodium/sugar cotransporter) member 9	
			Spata6	Spermatogenesis associated 6	
Head width (mm)	8	84.9 - 85.8	*Filip1*	Filamin A interacting protein 1	6q13-q14.3

Phenotype	Chromosome	Interval (Mb)	Gene symbol	Gene name	Human synteny
			Impg1	Interphotoreceptor matrix proteoglycan 1	
			Myo6	Myosin VI	
			Senp6	SUMO1/sentrin specific peptidase 6	
Femur length (mm)	10	45.7 - 47.1	*Alkbh5*	AlkB alkylation repair homolog 5 (E. coli)	1q42.1-q44
			Atpaf2	ATP synthase mitochondrial F1 complex assembly factor 2	17p11.2
			Cops3	COP9 signalosome subunit 3	
			Dhrs7b	Dehydrogenase/reductase (SDR family) member 7B	
			Drg2	Developmentally regulated GTP binding protein 2	
			Flcn	Folliculin	
			Flii	Flightless I homolog (Drosophila)	
			Gtlf3b	Gene trap locus F3b	
			Jmjd4	Jumonji domain containing 4	
			Llgl1	Lethal giant larvae homolog 1 (Drosophila)	
			Lrrc48	Leucine-rich repeat-containing protein 48	
			Map2k3	Mitogen activated protein kinase kinase 3	
			Med9	Mediator complex subunit 9	
			Mprip	Myosin phosphatase Rho interacting protein	
			Myo15a	Myosin XVA	
			Nlrp3	NLR family pyrin domain containing 3	
			Olr1462/1462/1464	Olfactory receptor 1462/1463/1464	
			Pld6	Phospholipase D family member 6	
			Rai1	Retinoic acid induced 1	
			Rasd1	RAS dexamethasone-induced 1	
			Shmt1	Serine hydroxymethyltransferase 1 (soluble)	
			Smcr7/8	Smith-Magenis syndrome chromosome region candidate 7/8	
			Snap47	Synaptosomal-associated protein 47	
			Srebf1	Sterol regulatory element-binding protein 1	
			Tmem11	Transmembrane protein 11	
			Tom1l2	TOM1-like protein 2	
			Top3a	Topoisomerase (DNA) III alpha	
			Zfp496/867	zinc finger protein 496/867	

Phenotype	Chromosome	Interval (Mb)	Gene symbol	Gene name	Human synteny
Femur neck ultimate force (N)	10	46.4 - 46.9	Alkbh5	AlkB alkylation repair homolog 5 (E. coli)	17p11.2
			Atpaf2	ATP synthase mitochondrial F1 complex assembly factor 2	
			Drg2	Developmentally regulated GTP binding protein 2	
			Flii	Flightless I homolog (Drosophila)	
			Llgl1	Lethal giant larvae homolog 1 (Drosophila)	
			Lrrc48	Leucine-rich repeat-containing protein 48	
			Myo15a	Myosin XVA	
			Rai1	Retinoic acid induced 1	
			Smcr7/8	Smith-Magenis syndrome chromosome region candidate 7/8	
			Srebf1	Sterol regulatory element-binding protein 1	
			Tom1l2	TOM1-like protein 2	
			Top3a	Topoisomerase (DNA) III alpha	
Femur elongation (mm)	11	41.4 - 44.3	Arl6	ADP-ribosylation factor-like 6	3q11.2-q13.33
			Cldnd1	Claudin domain containing 1	3q12-q26
			Cmss1	Cms1 ribosomal small subunit homolog (yeast)	
			Col8a1	Collagen type VIII alpha 1	
			Cpox	Coproporphyrinogen oxidase	
			Crybg3	Beta-gamma crystallin domain containing 3	
			Dcbld2	Discoidin CUB and LCCL domain containing 2	
			Epha6	Eph receptor A6	
			Filip1l	Filamin A interacting protein 1-like	
			Gabrr3	Gamma-aminobutyric acid (GABA) A receptor rho 3	
			Gpr15	G protein-coupled receptor 15	
			Mina	Myc induced nuclear antigen	
			Nit2	Nitrilase family member 2	
			Olr1 clusters	Olfactory receptors clusters	
			St3gal6	ST3 beta-galactoside alpha-23-sialyltransferase 6	
			Tbc1d23	TBC1 domain family member 23	
			Tmem30c	Transmembrane protein 30C	
Lumbar area (mm^2)	12	22.0 - 22.5	Ccl24/26	Chemokine (C-C motif) ligand 24/26	7q11.23
			Fkbp6	Peptidyl-prolyl cis-trans isomerase FKBP6	

Phenotype	Chromosome	Interval (Mb)	Gene symbol	Gene name	Human synteny
			Hip1	Huntingtin interacting protein 1	
			Mdh2	Malate dehydrogenase, mitochondrial	
			Nsun5	NOL1/NOP2/Sun domain family, member 5	
			Pom121	Nuclear envelope pore membrane protein POM 121	
			Por	NADPH-cytochrome P450 reductase	
			Rhbdd2	Rhomboid domain containing 2	
			Srrm3	Serine/arginine repetitive matrix 3	
			Styxl1	Serine/threonine/tyrosine-interacting-like protein 1	
			Tmem120a	Transmembrane protein 120A	
			Trim50	E3 ubiquitin-protein ligase TRIM50	
Neck width (mm)	17	89.0 - 89.8	*Arl5b*	ADP-ribosylation factor-like 5B	10p12.1-p13
			Cacnb2	Calcium channel voltage-dependent beta 2 subunit	
			Nsun6	NOP2/Sun domain family member 6	
Femur length (mm)	20	32.6 - 35.4	*Msl3l2*	Male-specific lethal 3-like 2	6q21-q22.33
			Tbc1d32	TBC1 domain family member 32	